BIOCHEMISTRY
including biophysical chemistry & molecular biology

Article

pubs.acs.org/biochemistry

# Modified Reactivity toward $O_2$ in First Shell Variants of Fet3p: Geometric and Electronic Structure Requirements for a Functioning Trinuclear Copper Cluster

Christian H. Kjaergaard,[†] Munzarin F. Qayyum,[†] Anthony J. Augustine,[†] Lynn Ziegler,[§] Daniel J. Kosman,*[,§] Keith O. Hodgson,[‡,†] Britt Hedman,[‡] and Edward I. Solomon*[,‡,†]

[†]Department of Chemistry, Stanford University, Stanford, California 94305, United States

[‡]Synchrotron Radiation Lightsource, SLAC, Stanford University, Stanford, California 94309, United States

[§]Department of Biochemistry, School of Medicine and Biomedical Science, State University of New York, Buffalo, New York 14214, United States

Supporting Information

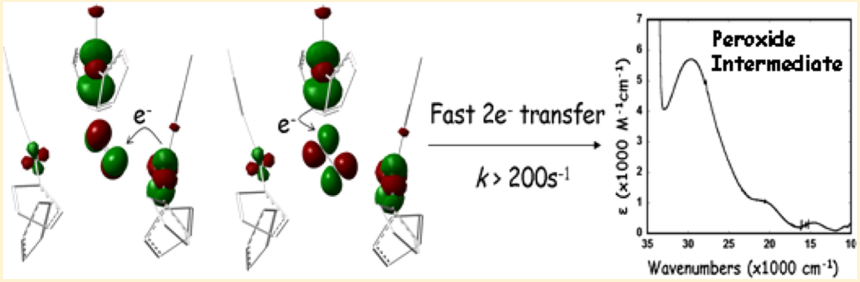


**ABSTRACT:** Multicopper oxidases (MCOs) carry out the most energy efficient reduction of $O_2$ to $H_2O$ known, i.e., with the lowest overpotential. This four-electron process requires an electron mediating type 1 (T1) Cu site and an oxygen reducing trinuclear Cu cluster (TNC), consisting of a binuclear type 3 (T3)- and a mononuclear type 2 (T2) Cu center. The rate-determining step in $O_2$ reduction is the first two-electron transfer from one of the T3 Cu's (T3$\beta$) and the T2 Cu, forming a bridged peroxide intermediate (PI). This reaction has been investigated in T3$\beta$ Cu variants of the Fet3p, where a first shell His ligand is mutated to Glu or Gln. This converts the fast two-electron reaction of the wild-type (WT) enzyme to a slow one-electron oxidation of the TNC. Both variants initially react to form a common T3$\beta$ Cu(II) intermediate that converts to the Glu or Gln bound resting state. From spectroscopic evaluation, the nonmutated His ligands coordinate linearly to the T3$\beta$ Cu in the reduced TNCs in the two variants, in contrast to the trigonal arrangement observed in the WT enzyme. This structural perturbation is found to significantly alter the electronic structure of the reduced TNC, which is no longer capable of rapidly transferring two electrons to the two perpendicular half occupied $\pi$*-orbitals of $O_2$, in contrast to the WT enzyme. This study provides new insight into the geometric and electronic structure requirements of a fully functional TNC for the rate determining two-electron reduction of $O_2$ in the MCOs.

MCOs catalyze the four-electron reduction of dioxygen to water, by oxidizing metal-ions and organic substrates, via a type 1 (T1) or blue copper site, which ranges in redox potential from ~350[1] to ~800 mV.[2] These electrons are transferred to a trinuclear copper cluster (TNC), comprised of a coupled binuclear T3 Cu- and a mononuclear T2 Cu center, which reduce dioxygen.[3] MCOs are found in all kingdoms of nature[4] and are involved in a number of functions, including iron homeostasis in mammals (ceruloplasmin)[5] and yeast (Fet3p),[6] and degradation of lignin in fungi (laccase).[7] The MCOs also have biotechnological applications,[8] including paper pulp bleaching[9] and bioremediation.[10] Additionally, much attention has been devoted to their incorporation into electrodes as biocathodes in devices such as implantable power sources and biosensors.[11,12] From a more fundamental perspective, MCOs have been intensively studied, primarily by a range of spectroscopic and kinetic techniques.[13,14] A main objective of these studies has been to elucidate the mechanism by which MCOs operate, in particular how the three spectroscopically defined Cu sites work in concert to achieve fast and energy-efficient reduction of dioxygen to water, coupled to four one-electron oxidations of substrates.

The spectroscopic characteristics of the three types of Cu sites in their resting oxidized form include an intense charge transfer (CT) transition in the absorption spectrum at ~600 nm and a small hyperfine $A_{par}$ value (~40−80 × $10^{-4}$cm$^{-1}$) in EPR for the T1 Cu,[15] a broad charge transfer (CT) absorption shoulder at ~330 nm originating from a bridging OH-ligand

**Received:** March 5, 2013
**Revised:** April 23, 2013
**Published:** April 30, 2013

that leads to antiferromagnetic coupling of the T3 Cu's (thus no EPR signal),[16] and a normal large $A_{par}$ value (~170−200 × $10^{-4}$cm$^{-1}$) and lack of an intense absorption band for the T2 Cu.[16]

The catalytic mechanism of MCOs can be divided into two parts (Scheme 1).[13,17,18] The first involves the binding of $O_2$ to the reduced TNC with four-electron transfer, generating the native intermediate (NI), where the O−O bond has been cleaved, but the product oxygens remain bound as bridging ligands in the TNC. The second part of the catalytic cycle involves the reduction of NI by a series of three electrons via the T1 Cu, regenerating the fully reduced TNC, followed by reduction of the T1 Cu, leaving a four-electron loaded enzyme ready for further $O_2$ reduction. Upon depletion of the reducing substrate, the catalytic cycle is arrested, and NI decays to the resting oxidized form of the enzyme.[19,20] The first part of the catalytic cycle, the $O_2$ binding and O−O bond cleavage, proceeds in two steps.[13,17,18] First, two electrons are transferred from the T2 and T3$\beta$ Cu's (the T3 Cu closest to a conserved aspartate residue (D94 in Fet3p) at the T3$\beta$-T2 edge, tuning down the redox potentials of both of these Cu's), to form the peroxide intermediate (PI).[21,22] Second, fast ET from the T1 Cu to the T2 Cu, activates the TNC for a second two-electron transfer (involving the T2 and T3$\alpha$ Cu sites) cleaving the O−O bond of PI to generate NI.[21] Both PI and NI have been trapped and spectroscopically characterized. PI can be trapped by mutation to form the type 1 depleted (T1D) derivative[23] or by chemical removal of the T1 Cu to form the T1 mercury substituted derivative (T1Hg).[24] The depletion of the T1 Cu leaves only one electron readily available at the TNC, and this greatly reduces the formation rate of NI from PI due to the slow one-electron reduction of peroxide.[25,26] Alternatively, with a functional T1 Cu, NI is rapidly formed upon exposure of the fully reduced enzyme to $O_2$ with no observation of PI. Importantly, the formation rate of PI in both the T1D and T1Hg derivatives is kinetically competent to be a precursor step in the formation of NI, indicating that the first two-electron transfer is rate determining in this four-electron reduction of $O_2$.[13,17] Indeed, the formation of NI is observed in the slow reduction of PI in the T1Hg derivative.[26]

**Scheme 1. Catalytic Cycle of MCOs**[a]

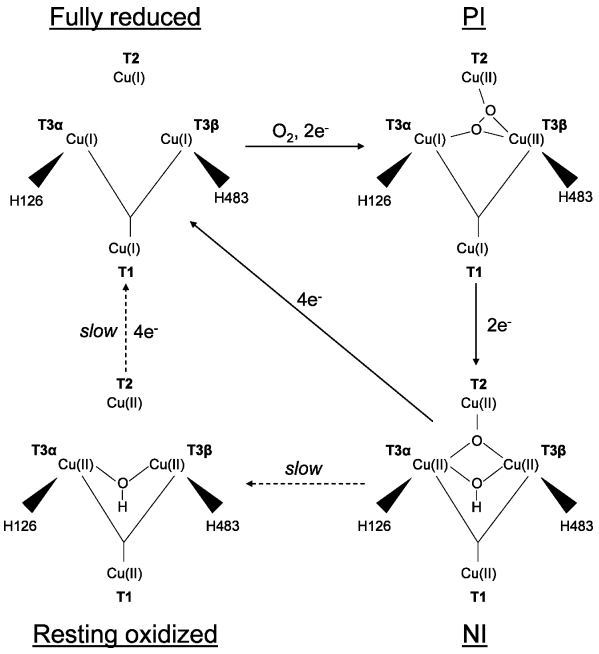


[a]The first part includes the four-electron reduction of $O_2$ to form NI, proceeding in two two-electron transfer steps, via PI. The second part includes four one-electron oxidations of substrate, regenerating the fully reduced enzyme. The decay rate of NI to the resting oxidized enzyme and the reduction rate of the resting oxidized to fully reduced enzyme are both too slow to be part of the catalytic cycle.

A detailed molecular mechanism for the second two-electron step, forming NI from PI, has been determined.[21] In contrast, little is known about the rate determining first two-electron step generating PI. In a recent study of first shell T3 Cu ligands in the MCO Fet3p,[22] we showed experimentally that the T2 and T3$\beta$ Cu(I)'s donate the first two electrons to $O_2$, in agreement with a computational evaluation of possible PI structures.[21] By mutating T3$\alpha$ and T3$\beta$ Cu His ligands to Gln in T1D Fet3p, the reduced T3$\alpha$ variant, T1DH126Q, formed PI in a rapid reaction with $O_2$, whereas no fast $O_2$ reactivity was observed for the T3$\beta$ variant, T1DH483Q. The spectroscopic features and formation rate of PI in the T3$\alpha$ variant were identical to those of WT T1D, consistent with the non-perturbed T3$\beta$ and T2 Cu's constituting the reactive edge of the TNC in the first two-electron transfer to $O_2$ in the MCOs.

Understanding the unique arrangement of the TNC, which enables the efficient rate determining reaction of the T2 and T3$\beta$ Cu's with $O_2$, is highly important. We have therefore extended the mutational studies of the Fet3p first shell residues to include the T3$\beta$ Cu variant, H483E. This mutation was chosen for its negatively charged side chain, which lowers the potential of the T3$\beta$ Cu. The reactivity of this variant is found to involve a slow one-electron reduction of $O_2$, in contrast to the fast two-electron reduction observed in the WT enzyme. Further, examination of the T1DH483Q variant on a longer time scale reveals an analogous but slower one-electron activity. From comparative spectroscopic studies, a detailed mechanism for this one-electron reaction with $O_2$ is elucidated. The difference in reactivity between the WT TNC and its T3$\beta$ variants is explained in terms of the orbital requirements for two-electron reduction of $O_2$ to form a bridged PI, thus providing novel insight into how ligation and geometry program the TNC for this essential two-electron $O_2$ reduction.

## 1. MATERIALS AND METHODS

All chemicals were minimum reagent grade or higher and used without further purification. MES buffer was purchased from Genscript. All other chemicals were purchased from Sigma. Water was purified on a Nanopure Diamond purifier from Barnstead to a resistivity of >17MΩ cm$^{-1}$.

The mutant FET3 alleles were constructed directly in pDY148 by site directed mutagenesis using the QuickChange kit from Strategene. WT T1D and H483E mutants were generated using complementary primers in PCR amplification of the vector. The double mutants, T1DH483E and T1DH483Q were generated in two sequential rounds of mutagenesis. Sequences of Fet3p mutants were confirmed by automated fluorescence sequencing using an ABI PRISM 377 instrument. The vectors expressing the mutant proteins were transformed into yeast strain M2* for soluble protein expression. WT, T1D, H483E, T1DH483E, and T1DH483Q mutant proteins were expressed, isolated, and purified as previously described. Purified protein was characterized by the Bradford dye-binding assay[27] and the 2,2-biquinoline assay,[28]


dx.doi.org/10.1021/bi4002826 | Biochemistry 2013, 52, 3702−3711

for protein concentration and copper content determination, respectively.

UV−visible (UVvis) absorption spectra were acquired on an Agilent 8453 diode array spectrophotometer, in the energy range from 190 to 1100 nm. EPR spectra were obtained with a Bruker EMX spectrometer, an ER 041 XG microwave bridge, and an ER4116DM cavity. A sample temperature of 77 K was maintained using a liquid nitrogen finger dewar. EPR settings were as follows: freq. ≈ 9.6 GHz, power ≈10 mW, rec. gain = $5.02 \times 10^3$, mod. freq. = 100 kHz, mod. amp. = 10.00G, time constant = 327.68 ms, conversion time = 81.92 ms, and sweep time = 83.89 s. All spectra were averaged over 3 scans. EPR simulations were done using SIMPOW6 software.[29] EPR spin quantitation of the paramagnetic copper content was performed using a 1.0 mM standard solution of $CuSO_4 \cdot 5H_2O$, 2 mM HCl, and 2 M $NaClO_4$. Magnetic circular dichroism (MCD) spectra were measured on a Jasco J-810-150S spectrapolarimeter with an S-20 photomultiplier tube coupled to an Oxford SM4000-8T magnet in the UVvis region. In the near-IR region, MCD spectra were measured with either a Jasco 200-D or J-730 spectrapolarimeter and a liquid nitrogen cooled InSb detector coupled either to an Oxford SM4000-7T or SM40008T magnet. MCD samples were prepared in deuterated MES buffer at pD 6.0 and mixed with 50% (v/v) glycerol-d3, to obtain high quality glasses. The MCD cells have two quartz disks sealed with a 3-mm rubber spacer. Zero-field baseline effects were eliminated in MCD by taking an average of the +7 and −7 T scans, [7 − (−7)]/2 T. Gaussian fitting of the MCD data was done using PeakFit 4.0 (Jandel).

Cu K-edge X-ray absorption spectra were measured at XAS stations BL9-3 (focused) and BL7-3 (unfocused) at the Stanford Synchrotron Radiation Lightsource (SSRL) under 3 GeV and 80−350 mA storage ring operating conditions. Energy selection was attained using a Si(220) double-crystal monochromator. A Rh-coated premonochromator collimating and harmonic rejection mirror was used for both beamlines. A cylindrical Rh-coated bent postmonochromator mirror was also used on BL9-3 for focusing. Protein samples were loaded into Lucite cells with Kapton windows. The samples were immediately frozen and stored under liquid nitrogen. An Oxford Instruments CF1208 liquid He continuous-flow cryostat held samples at a constant temperature of 10 K during XAS measurement. Data were measured in fluorescence mode using a Canberra Ge 30-element array detector. Internal energy calibration was accomplished by simultaneous measurement of the absorption of a Cu-foil placed between two ionization chambers situated after the sample. The first inflection point of the foil spectrum was assigned to 8980.3 eV. The energy-calibrated data from 8675 to 9350 eV ($k$ = 9.5 Å$^{-1}$) were processed by fitting a second-order polynomial to the pre-edge region and subtracting this from the entire spectrum as a background. Normalization of the data was achieved by scaling the postedge data to 1.0 at 9,000 eV. This background subtraction and normalization was done using PySpline.[30] For each sample, several scans from 8675 to 9350 eV were collected and normalized in PySpline. Several faster scans from 8970 to 9020 eV were also collected for the oxidized samples to minimize photoreduction in the beam. Subsequent scans collected over time on the same sample spot revealed an isosbestic point around ∼8994 eV. The postedge of the shorter scans were normalized in KaleidaGraph by maintaining the same isosbestic point as the data normalized using PySpline[30] of the 8675−9350 eV scans. The pre-edge of the shorter scans were processed to match the pre-edge of the longer PySpline-processed data. Data presented here are the first scans of each data set to eliminate spectral changes from photoreduction.

Reduced protein was obtained by argon purging for ∼4 h followed by the addition of excess dithionite in a Vacuum Atmosphere glovebox. Complete reduction of the protein was confirmed by EPR and UVvis absorption spectroscopies. Prior to reoxidation, excess dithionite was removed in the glovebox by buffer exchange into degassed MES buffer using 10K Amicon Ultra centrifugal filters from Millipore. Reoxidation experiments were performed by mixing fully reduced protein with oxygenated buffer. The reoxidation process was followed by continuous UVvis monitoring and through EPR and XAS spectra of $LN_2$ quenched samples obtained at various time points.

DFT calculations were performed using the Gaussian 09 software package.[31] The starting point of the geometry optimized structures was obtained from the coordinates of the Fet3p crystal structure (1ZPU). The first sphere His ligands were truncated by replacing the $\alpha$-C by H's. These hydrogens were frozen along with the hydrogens of the noncoordinating His-N's. The geometry optimization was performed using the B3LYP functional and TZVP basis sets on all atoms. Solvation effects were included with the polarized continuum model as implemented in Gaussian 09 with a dielectric constant of 4.0. Orbital contours were visualized with Gaussview.

## 2. RESULTS AND ANALYSIS

### 2.1. Isolation and Characterization of T1DH483E.

*2.1.1. As-Isolated T1DH483E.* The T3$\beta$- ligand, H483 of the TNC, was mutated to glutamate (E) and expressed in the holo (i.e., with T1 Cu ligands intact)- and T1-depleted forms, H483 and T1DH483E, respectively. A detailed characterization of the holo H483E variant is given in Supporting Information (Figures S1−S4). The spectroscopic features of the holo and T1D H483Q variants are described in ref 22. Here, we focus on the T1DH483E variant of Fet3p. Elimination of the T1 Cu in both the T1DH483E and Q variants allow for the spectroscopic features of the TNC to be characterized and the initial reaction of reduced Fet3p enzyme with $O_2$ to be monitored.

From Biorad and Biquinoline assays, as-isolated T1DH483E incorporates 2.9 Cu/enzyme, verifying that Cu does not bind at the T1 site. This correlates with the lack of 610 nm intensity observed in the absorbance spectrum (Figure 1a). The 330 nm band observed in the WT T1D enzyme is also absent, indicative of a perturbed TNC in the T1DH483E variant. The EPR spectrum of T1DH483E (Figure 1b) shows features from a single paramagnetic Cu(II) in the TNC with a spin integration of 0.9 Cu/enzyme. The EPR spectrum can be simulated with $g_z$ = 2.286, $A_z = 158 \times 10^{-4}$ cm$^{-1}$, $g_y$ = 2.079, $A_y = 25 \times 10^{-4}$ cm$^{-1}$, $g_x$ = 2.052, and $A_x = 14 \times 10^{-4}$ cm$^{-1}$ (Figure S5, Supporting Information), consistent with a slight rhombically distorted tetragonal Cu geometry with $g_z > g_y, g_x$. The EPR spectrum of the Cu(II) of the TNC in the T1DH483E variant is markedly different from that of the WT T1D enzyme ($g_z$ = 2.243, $A_z = 190 \times 10^{-4}$ cm$^{-1}$, $g_y$ = 2.055, $A_y = 17 \times 10^{-4}$ cm$^{-1}$, $g_x$ = 2.041, and $A_x = 15 \times 10^{-4}$cm$^{-1}$), previously assigned to the T2 Cu(II) (Figure 1b, dashed line). This indicates that a different Cu is paramagnetic in the TNC of T1DH483E, compared to the WT enzyme.

The redox state of the TNC in as-isolated T1DH483E was evaluated by Cu K-edge XAS, probed by the intensity of the 8984 eV feature correlated to reduced Cu. As observed in


dx.doi.org/10.1021/bi4002826 | Biochemistry 2013, 52, 3702−3711

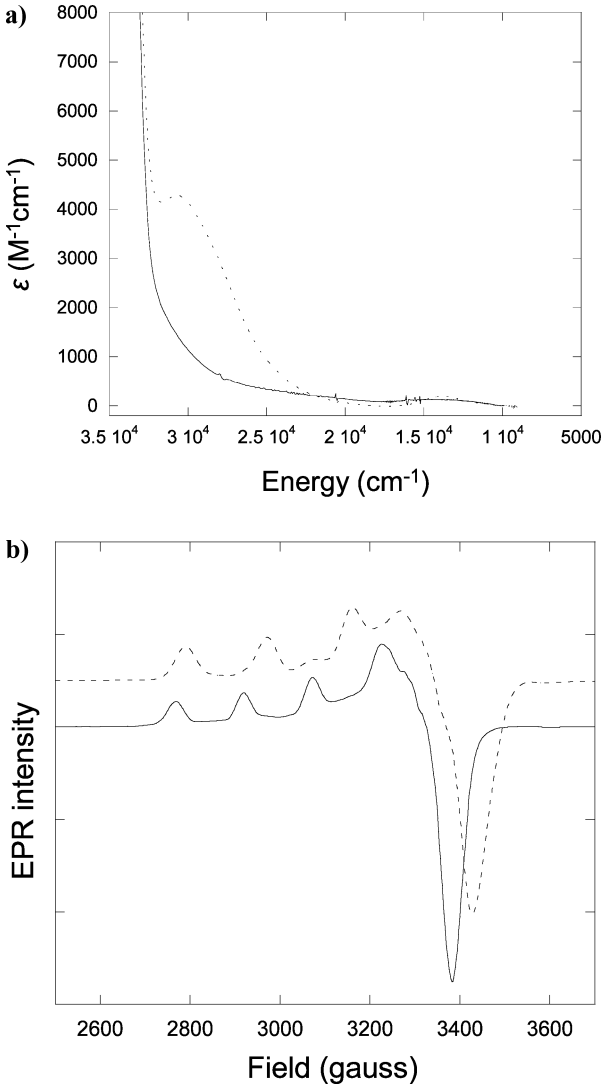


**Figure 1.** (a) UVvis absorbance spectrum of as-isolated T1DH483E (solid line). The spectrum of WT T1D in the resting enzyme form (dotted line) is included as reference. MES buffer, pH 6.0. (b) EPR spectrum of as-isolated T1DH483E (solid line) and WT T1D in the resting enzyme form (dashed line). MES buffer, pH 6.0.

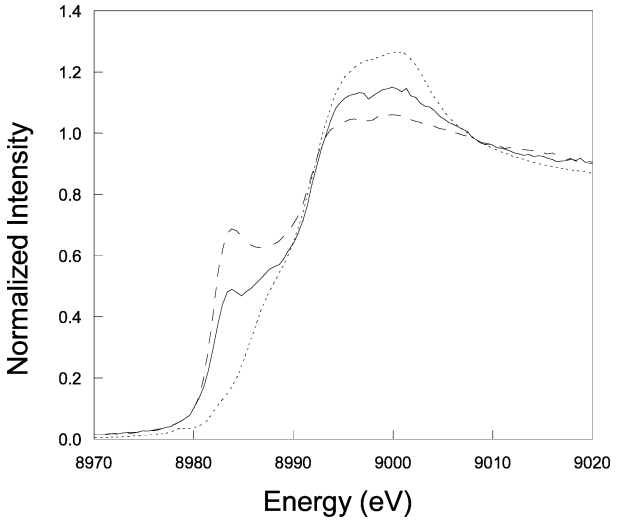


**Figure 2.** Cu K-edge XAS spectrum of as-isolated T1DH483E (solid line). Resting WT T1D (dotted line), i.e., fully oxidized and reduced WT T1D (dashed line), is included as reference. MES buffer, pH 6.0.

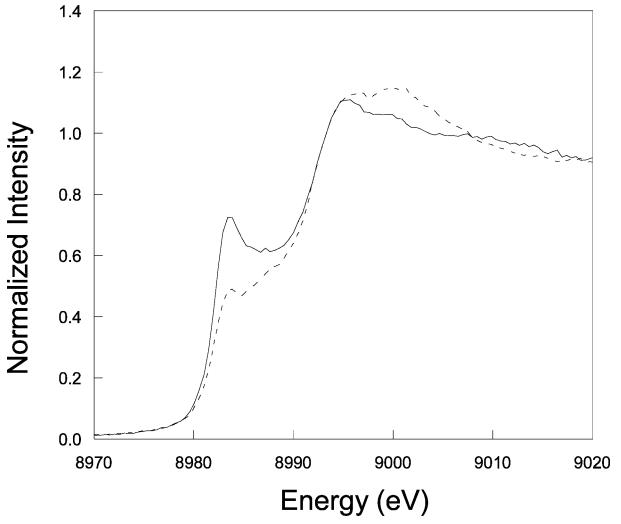


**Figure 3.** Cu K-edge XAS spectrum of fully reduced T1DH483E (solid line). As-isolated T1DH483E (dashed line) is included as reference. MES buffer, pH 6.0.

Figure 2, the TNC in T1DH483E is ~60% reduced, based on a comparison with the fully reduced and fully oxidized WT T1D. This result allows for the assignment of the TNC of T1DH483E to 1× Cu(II), 2× Cu(I), which is in agreement with the EPR and absorption results.

*2.1.2. Reduced T1DH483E- Cu K-edge XAS.* The shape of the 1s → 4p transition at ~8984 eV is sensitive to the geometry of the Cu(I) ion and from a comparison to a library of Cu(I) sites with known geometries,[32] the coordination environment of a Cu(I) site can be evaluated. The experimental XAS spectrum of fully reduced T1DH483E (Figure 3) has a normalized value of 0.73 for the 8984 eV feature. This is more intense than the corresponding peak in the fully reduced WT T1D (Figure 2), indicating a change in geometry of the reduced Cu's of the TNC in T1DH483E compared to those of the WT T1D enzyme. To determine the geometry change upon reduction of the single oxidized TNC Cu in as-isolated T1DH483E, fits of the fully reduced spectrum were obtained by subtracting 1xCu(II) from the as-isolated spectrum (i.e., containing 1xCu(II) and 2xCu(I)), and substituting it with 1xCu(I) from the library of model complexes. The best fits were achieved with a linear two-coordinate Cu(I) or a linear Cu(I) site with a weakly bound third ligand, whereas nonlinear three- and four-coordinate Cu(I) sites result in too low an intensity in the 8984 eV region (Figure S6, Supporting Information). Therefore, in the T1DH483E variant, the mutated His to Glu ligand is no longer capable of binding to the T3$\beta$ Cu in the reduced state, which results in the nonmutated His ligands, H128 and H418, adapting a close to linear conformation. This is in contrast to the WT Fet3p, where the crystal structure reveals a trigonal pyramidal geometry of the T3$\beta$ Cu(I).[33] The geometry change observed in the T1DH483E variant compared to the WT T1D enzyme is consistent with the behavior of T1DH483Q, found in our previous study.[22]

**2.2. Reactivity of Reduced T1DH483E with $O_2$.** *2.2.1. Reoxidation of the TNC in T1DH483E.* The first facile two-electron transfer from a fully reduced TNC to dioxygen has been studied in the type 1 depleted variant, where the


dx.doi.org/10.1021/bi4002826 | *Biochemistry* 2013, 52, 3702−3711

elimination of the T1 electron allows for trapping of PI. In Fet3p, it was previously found that WT T1D as well as the T3$\alpha$-variant, T1DH126Q, formed PI, whereas no fast $O_2$ reaction was observed with fully reduced T1DH483Q.[22] Formation of PI in the reaction of $O_2$ with fully reduced T1DH483E was evaluated by absorbance, Cu K-edge XAS, and EPR. From the absorbance difference spectrum of fully reduced T1DH483E before and immediately following the addition of $O_2$ (Figure 4), no absorption at ~30,000 $cm^{-1}$ is observed,

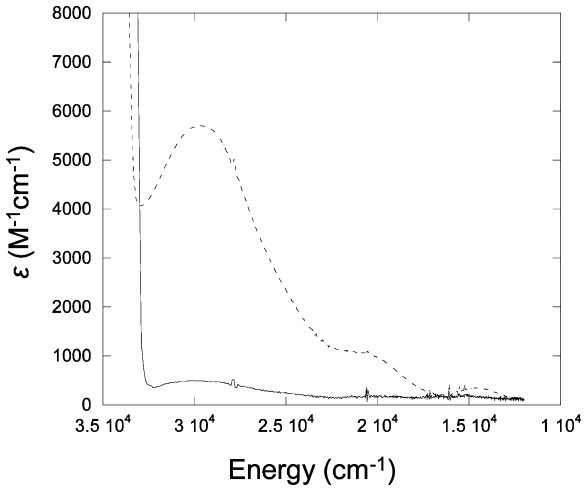


**Figure 4.** UVvis absorbance difference spectra of T1DH483E in the reduced form subtracted from T1DH483E reoxidized with $O_2$ for 30 s (solid line). Corresponding difference spectrum for WT T1D (dashed line). MES buffer, pH 6.0.

consistent with the lack of PI formation. To detect possible oxidation events, not detectable by absorbance, the reaction was monitored by Cu K-edge XAS. As observed in Figure 5a, no significant change occurs in the 8984 eV region within the first 30 s of $O_2$ addition to reduced T1DH483E (overlaying black and red lines), indicating that oxidation of the TNC does not occur in this time frame. This is in contrast to WT T1D, where this intensity decreases by more than 60% within the first 30 s (Figure 5b), reflecting the rapid two-electron reduction of $O_2$ to form PI. Importantly, when reduced T1DH483E is allowed to react with $O_2$ over extended times (>15 h), the 8984 eV feature in the XAS spectrum eventually decreases to the level of the as-isolated enzyme (Figure 5a, green and blue line), indicating oxidation of a single Cu of the TNC. Thus, the mutation of the T3$\beta$ Cu ligand H483 to E converts the $O_2$ reactivity from facile two-electron oxidation to a slow one-electron oxidation of the TNC.

The slow one-electron oxidation of the TNC in T1DH483E was monitored by EPR (Figure 6), allowing for the kinetics of this process to be determined by integration of the spin intensities at various time-points (Figure 6, insert). A reasonable fit to the EPR intensities can be obtained with a first order reaction rate of $5.6 \times 10^{-2}$ $min^{-1}$, more than 5 orders of magnitude slower than the facile two-electron oxidation rate of WT T1D (~200 $s^{-1}$).[23] Inspection of the time-dependent EPR spectra reveals that the reoxidation of the TNC proceeds via an intermediate species (Figure 6, solid blue line) that slowly decays to the final form (Figure 6, solid red line) with the same EPR features as those of the as-isolated T1DH483E enzyme (Figure 6, dashed green line). Simulated spectra (Figures S7 and S5, Supporting Information) of the

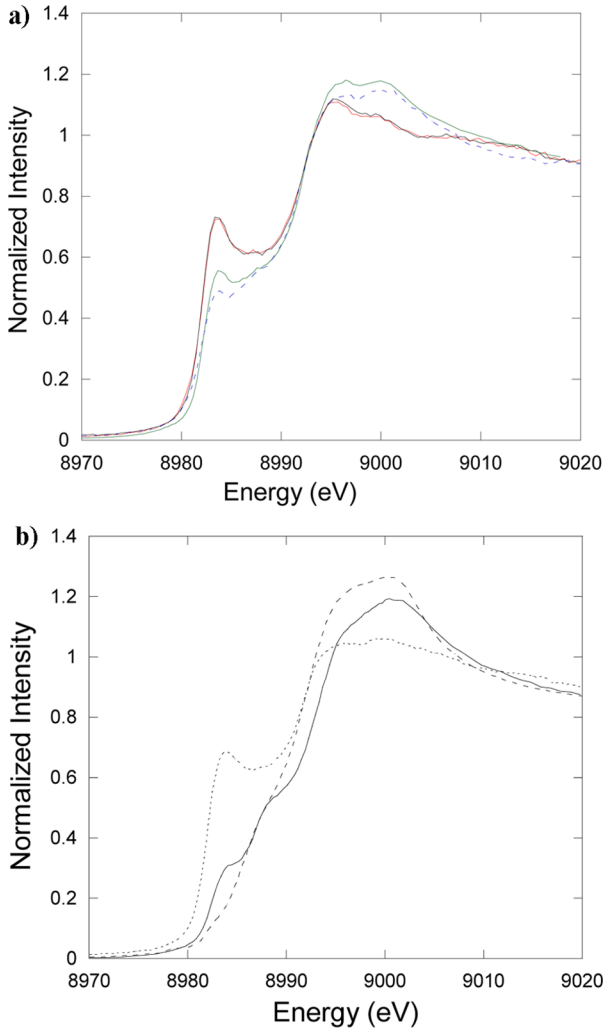


**Figure 5.** (a) Cu K-edge XAS spectra of T1DH483E: fully reduced (red), reoxidized for 30 s (black), reoxidized for 45 h (green), and as-isolated (blue). The additional intensity at 8984 eV in the 45 h reoxidized spectrum, in comparison to as-isolated enzyme, is due to ~15% unreacted enzyme. MES buffer, pH 6.0. (b) Cu K-edge XAS spectra of WT T1D: fully reduced (dotted line), reoxidized for 30 s (solid line), and as-isolated, i.e., fully oxidized (dashed line). MES buffer, pH 6.0.

intermediate and final forms were used to generate the time-dependent speciation of the reoxidation process (Figure 7). Kinetic fitting of this speciation is consistent with the kinetic model in eq 1:

$$\text{fully reduced (3xCu(I))} \xrightarrow{k_1} \text{intermediate (2xCu(I), 1xCu(II))} \xrightarrow{k_2} \text{final form(2xCu(I), 1xCu(II))} \quad (1)$$

with rate constants of $k_1 = 5.6 \times 10^{-2}$ $min^{-1}$ and $k_2 = 7 \times 10^{-4}$ $min^{-1}$.

*2.2.2. Oxidation of Reduced T1DH483Q: Comparison with T1DH483E.* From our previous study, reaction of reduced T1DH483Q with $O_2$ did not lead to fast PI formation as evaluated by absorbance spectroscopy.[22] This is consistent with the lack of change in the Cu K-edge XAS spectra of reduced T1DH483Q before and immediately after reaction with $O_2$. (Figure S8, Supporting Information). We now extend the


dx.doi.org/10.1021/bi4002826 | *Biochemistry* 2013, 52, 3702−3711

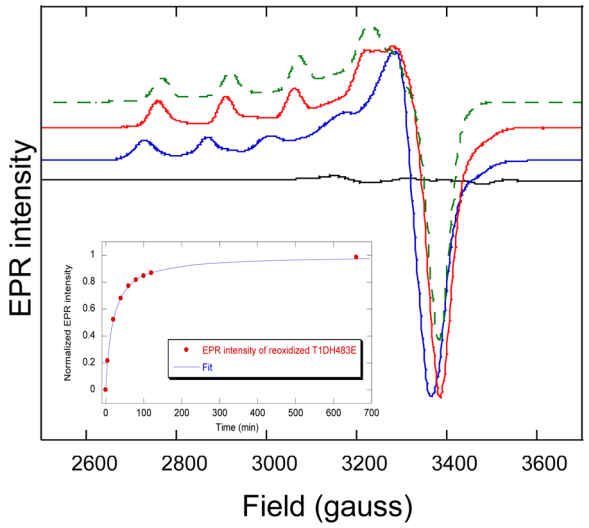


**Figure 6.** Reoxidation of reduced T1DH483E at 30 s (black), 40 min (blue), 45 h (red). The as-isolated enzyme (green, dashed line) is included for comparison. Insert: Reoxidation of T1DH483E TNC evaluated by spin integration of time-dependent EPR spectra (red circles). First order fit of reoxidation (blue, solid line), $k$ = 0.05 $min^{-1}$. MES buffer, pH 6.0.

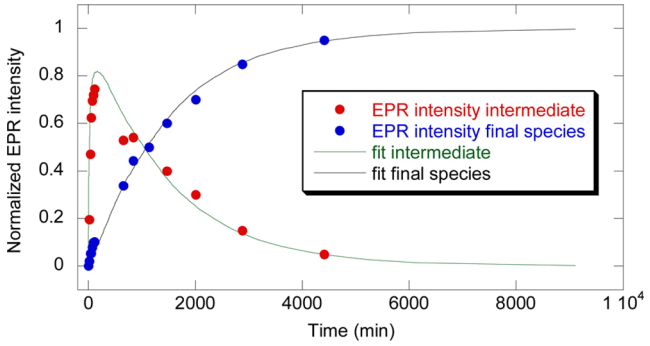


**Figure 7.** Speciation of intermediate (red circles) and final forms (blue circles) of T1DH483E TNC evaluated by spin integration of time-dependent EPR spectra. Fit of intermediate (green, solid line) and final forms (black, solid line).

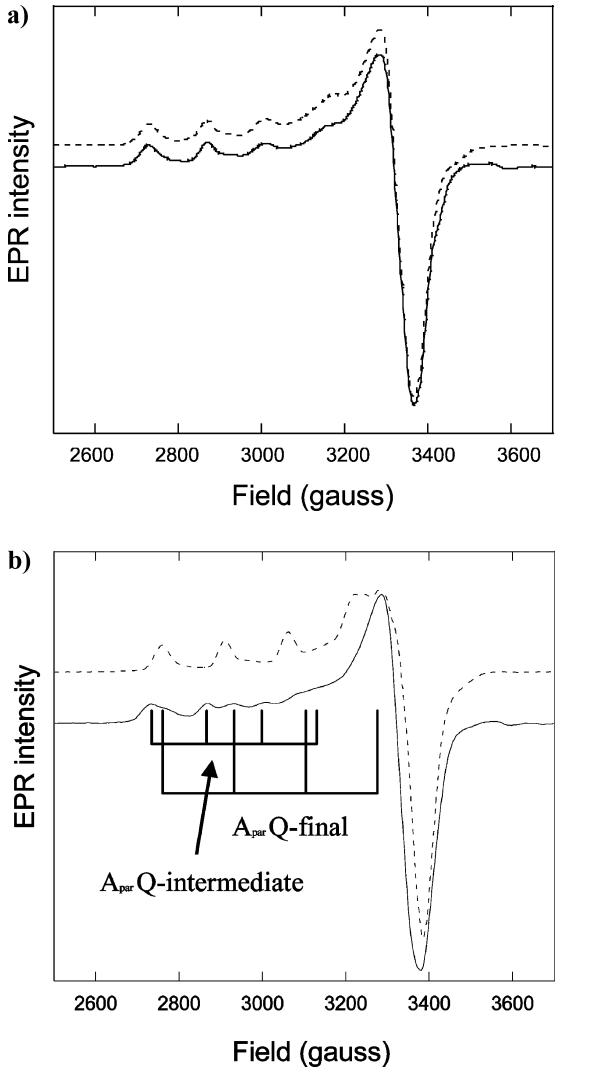


**Figure 8.** (a) EPR spectra of intermediate reoxidized T1DH483Q (solid line) and T1DH483E (dashed line) (blue line, Figure 6). MES buffer, pH 6.0. (b) EPR spectra of reoxidized T1DH483Q (solid line) and T1DH483E (dashed line) (red line, Figure 6) at 45 h. $A_{par}$ hyperfine lines are indicated for the intermediate and final forms of T1DH483Q. MES buffer, pH 6.0.

investigation of the $O_2$ reactivity of this variant to long time periods, for comparison to the $O_2$ reactivity of reduced T1DH483E. As for T1DH483E, EPR spectroscopy shows a slow one-electron reoxidation of the Q variant with initial formation of an intermediate species (Figure 8a) which decays to a final species (Figure 8b) with EPR features similar to the minor species in the as-isolated T1DH483Q enzyme (Figure S9, Supporting Information). The kinetic trace of reoxidation for this variant (Figure S10, Supporting Information) can be fit with a $k_1$ rate constant of 1.3 × $10^{-2}$ $min^{-1}$ (eq 1), which is more than 4-fold slower than for the T1DH483E Fet3p variant. ($k_2$ could not be determined due to the degradation of T1DH483Q at these extended times.) By comparison of the EPR features of the initially reoxidized species in T1DH483E and Q (Figure 8a), both variants oxidize to form the same intermediate before they decay to two different final species (Figure 6 and 8b).

*2.2.3. Mechanism of the Oxidative Reactivity in the T1DH483 Variants.* The data above reveal that both T1DH483E and Q variants undergo slow one-electron oxidation of the TNC via a common intermediate, before decaying to their respective resting enzyme species, with the reoxidation of T1DH483E being more than four times faster than that for the T1DH483Q variant. The identical EPR features of the intermediates for the two variants argue against either mutated residue being coordinated to the Cu(II) of this species. Also, the markedly different EPR parameters of the intermediate (Figure 8a), compared to those of the T2 Cu(II) observed in WT T1D (Figure 1b), show that the T2 Cu is not the oxidized Cu in the intermediate. Finally, the difference in oxidation rates of T1DH483E compared to Q indicates that these rates are modulated by residue type at amino acid 483, a ligand to T3$\beta$. The elevated oxidation rate for the Glu over the Gln variant is consistent with having the negatively charged residue in the vicinity of the redox active T3$\beta$ Cu. These results argue for a slow one-electron oxidation of the reduced TNC in the variants with formation of a common T3$\beta$ Cu(II) intermediate that decays to two different final species reflecting recoordination of the different side chain residues at position 483.


dx.doi.org/10.1021/bi4002826 | *Biochemistry* 2013, 52, 3702−3711

**2.3. MCD and EPR Spectra of Intermediate and Resting Species.** Insight into the electronic and geometric structures of the intermediate and final Cu(II) sites can be obtained from a correlation of the MCD and EPR data as these directly reflect the ligand field of this Cu.[34] Figure 9 shows the

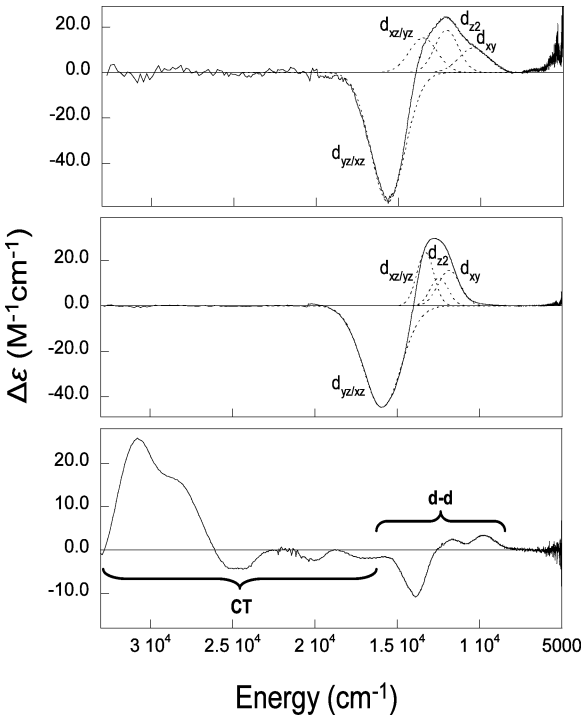


**Figure 9.** Experimental LT-MCD spectra of the T1DH483E intermediate (top) and its final form (middle). WT T1D (T2 Cu(II)) (bottom) is included for comparison. Gaussian fits of the intermediate and final forms are included (dotted line). Deuterated MES buffer, pD 6.0 with 50% (v/v) glycerol-d3.

LT-MCD spectrum of the intermediate in the T1DH483E variant in the Fet3p as well as the MCD spectrum of the final species. (The MCD features of the T1DH483Q intermediate (not shown) are identical to those of the T1DH483E intermediate, while the MCD of the final form of T1DH483Q was not obtained due to enzyme degradation (vide supra).) Gaussian fits of the MCD spectra are included in Figure 9, with the peak positions listed in Table 1. The LT-

**Table 1. Energies of LT-MCD Transitions for T1DH483E/Q Intermediate and T1DH483E Final Forms Obtained from Gaussian Fits**

| band | intermediate ($cm^{-1}$) | final ($cm^{-1}$) |
|---|---|---|
| 1. $d_{xy}$ | 10,444 | 11,830 |
| 2. $d_{z2}$ | 12,066 | 12,508 |
| 3. $d_{xz/yz}$ | 13,467 | 13,305 |
| 4. $d_{yz/xz}$ | 15,644 | 15,930 |

MCD spectrum of the T1DH483E intermediate form (Figure 9 (top)) can be fit with a total of four Gaussian bands in the energy region from 10,444 to ~15,644 $cm^{-1}$. No transitions are observed at higher energies. Similarly, for the final species formed (Figure 9, middle), four Gaussian bands can be resolved between 11,830 and 15,930 $cm^{-1}$, with no transitions at higher energies. For comparison, the LT-MCD spectrum of WT T1D, corresponding to the paramagnetic T2 Cu(II) site, is included in Figure 9 (bottom). In WT T1D, the d-d manifold is shifted to lower energy by ~1000−2000 $cm^{-1}$ compared to the variants. Also, low-energy charge transfer (CT) transitions, starting at ~16,700 $cm^{-1}$, are observed. Those spectral features reflect the three-coordinate nature of the T2 Cu(II) in the resting form of the MCOs.[35] Studies on model complexes show that in going from three-coordinate to four- or higher coordinate Cu(II) sites, the CTs shift up in energy by more than 6,000 $cm^{-1}$.[36] This allows the assignment of the intermediate and the final forms of T1DH483E as four (or higher) coordinate Cu(II) species. Thus, water derived ligands are present at the T3$\beta$ Cu(II), in addition to the ligated His amino acid residues H128 and H418 (and E483 in the final form).

The EPR spin Hamiltonian parameters for the intermediate and final species of T1DH483E and Q are listed in Table 2 with

**Table 2. EPR Parameters of the Intermediate and Final Forms of T1DH483E/Q**

| | intermediate | T1DH483E final | T1DH483Q final[a] |
|---|---|---|---|
| $g_{par}$ | 2.326 | 2.286 | ~2.26 |
| $g_{perp}$ | 2.06 | 2.05−2.08 | ~2.06 |
| $A_{par}$ | 149 × $10^{-4}cm^{-1}$ | 158 × $10^{-4}cm^{-1}$ | ~170 × $10^{-4}cm^{-1}$ |

[a]The values are estimated from the plot in Figure 8b.

$g_z > g_{x,y}$, corresponding to $d_{x^2-y^2}$ ground states associated with tetragonal structures. The excited state energy ordering of tetragonal Cu(II) sites is generally found to be $d_{x^2-y^2} \rightarrow d_{xy} < d_{z^2} < d_{xz} \approx d_{yz}$ (hole transitions indicated). The close to degenerate $d_{xz/yz}$-derived states form a derivative shaped pseudo-A-term feature in the LT-MCD spectrum due to their large spin orbit coupling.[34] This allows for the assignment of the four transitions observed in the MCD spectra of the two T1DH483E forms (Figure 9 and Table 1). The major difference between the final and intermediate forms is the increase in energy of the $d_{xy}$ to $d_{x^2-y^2}$ transition in the former. This shift in $d_{xy}$ energy affects the $g_{par}$ value, which in turn affects the $A_{par}$ value according to eqs 2 and 3

$$g_{par} = 2.0 - (8\lambda\alpha^2\beta^2/(E_{xy} - E_{x^2-y^2})) \quad (2)$$

$$A_{par} = Pd(-\kappa - 4/7 + (g_{par} - 2.0) + 3/7(g_{perp} - 2.0)) \quad (3)$$

where $\lambda$ (−830 $cm^{-1}$ for Cu(II)) is the spin−orbit coupling constant of Cu(II), $\alpha^2\beta^2$ is the metal character of the ground and excited states, $E_{xy} - E_{x^2-y^2}$ is the transition energy in the MCD, and $Pd(-\kappa - 4/7)$ are the Fermi contact and spin dipolar coupling contributions to the parallel hyperfine, which are large and negative for tetragonal Cu(II) species.[37] The increase in energy of the $d_{xy}$ to $d_{x^2-y^2}$ transition in going from the intermediate to the final form fully accounts for the observed decrease in $g_{par}$ and increase in $A_{par}$ (Table 2). The higher energy d-d transition in the final form of T1DH483E reflects weaker $\pi$-donation and therefore a less destabilized $d_{xy}$ state, as compared to the intermediate. As described above, decay of the intermediate to the resting form is consistent with recoordination of the glutamate side chain. Glutamate replacing a hydroxide ligand, in the intermediate, is therefore a valid model for this rearrangement, as the hydroxide is a stronger $\pi$-donating ligand. The validity of this model is supported by the


dx.doi.org/10.1021/bi4002826 | Biochemistry 2013, 52, 3702−3711

EPR data of the T1DH483Q variant. Here, the decay of the intermediate results in recoordination of a glutamine side chain, with the associated EPR spectrum showing a decrease in $g_{par}$ and increase in $A_{par}$ (Table 2), compared to the intermediate T1DH483E and Q forms and the final form of T1DH483E. This indicates stabilization of the $d_{xy}$ level in T1DH483Q consistent with the $\sigma$-donor nature of the glutamine carboxamide side chain.[38]

## 3. DISCUSSION

From spectroscopic evaluation, the T3$\beta$ variant T1DH483E in Fet3p is expressed with full Cu loading in a two electron reduced/one electron oxidized TNC. In contrast, the WT T1D enzyme is isolated with the TNC in its fully oxidized state. Cu K-edge XAS further shows that upon reduction of the single Cu(II) in the TNC of the T1DH483E derivative of Fet3p, the mutated ligand no longer coordinates to the T3$\beta$ Cu, resulting in linear arrangement of the two remaining His residues, H128 and H418. This is in contrast to the WT enzyme, where the three His ligands all coordinate to the reduced T3$\beta$ Cu forming a trigonal plane with the Cu situated slightly above that plane.[33] Importantly, when the fully reduced T1DH483E variant is exposed to $O_2$, only a slow one-electron oxidation of the TNC is observed, as opposed to the fast two-electron oxidation generating the peroxide intermediate in the WT T1D enzyme. T1DH483Q, previously found to be incapable of fast two-electron transfer,[22] is now shown to also undergo a slow one-electron oxidation of the TNC. EPR spectra indicate that the one-electron reoxidations of T1DH483E and Q proceed via a common intermediate that decays to different final Cu(II) structures. Also, the reoxidation rate of T1DH483E is significantly faster than that of T1DH483Q, a difference correlated to the negative charge of the carboxylate in the former leading to a decreased reduction potential of the T3$\beta$ Cu. On the basis of the XAS, EPR, and LT-MCD data on the intermediate and final forms of T1DH483E and Q, the $O_2$ reactions of the fully reduced TNCs of the T3$\beta$ variants proceed with oxidation of the T3$\beta$ Cu to form a tetragonal Cu(II) intermediate species with two nonmutated His ligands and two water derived ligands. This is followed by recoordination of the mutated E or Q residue, resulting in final species again with tetragonal ligand fields but with EPR parameters consistent with E vs Q coordination. The linear arrangement of the nonmutated T3$\beta$ Cu His ligands, H128 and H418, observed in the reduced and intermediate oxidized states of the variants relative to the WT TNC, reveals a high degree of flexibility in the first coordination sphere of residues upon mutation of H483. This reflects the fact that the backbones of H128 and H418 are part of loop regions, whereas the backbone of H483 is part of a more rigid $\beta$-sheet structure (Figure S11, Supporting Information). This flexibility is not observed in WT MCOs, where the trigonal arrangement of the T3$\beta$ Cu is conserved, as evident by the numerous crystal structures available of MCOs.

Our previous studies showed that in WT T1D the T3$\beta$ Cu is involved (along with the T2 Cu) in the first two-electron transfer to $O_2$, resulting in PI formation,[21,22] the rate determining step in four-electron reduction of $O_2$ to form NI in the native enzyme. This requires that the T3$\beta$ Cu is redox active and capable of binding exogenous ligands. Both of these requirements are fulfilled in the T1DH483E and Q variants of Fet3p in that the T3$\beta$ autooxidizes to an intermediate structure with water-derived ligands present. Considering the thermodynamic favorability of the two vs one-electron reduction of $O_2$ (+0.28 V vs −0.33 vs NHE at pH 7),[39] it is significant that the perturbed TNCs of the two variants only undergo one-electron redox chemistry. This shows that while the perturbed T3$\beta$ Cu is redox active in both variants, it is no longer able to participate, along with the T2 Cu, in a concerted two-electron transfer to form PI. To understand this difference in reactivity between the WT enzyme and the variants, valuable insight can be obtained from spectroscopically calibrated DFT calculations. Figure 10a shows geometry optimized DFT structures of the reduced TNC in the WT enzyme and the variants (without the H483 ligand, consistent with XAS Cu K-edge data). The overall arrangement of the His ligands and the Cu ions are conserved between the two forms. The main structural perturbation, upon elimination of the H483 ligand, is an increase in the T3$\beta$-Cu N(H128)−Cu-N(H418) angle from 113° in WT to 145° in the calculated variants. This behavior is in agreement with the experimentally defined close-to-linear arrangement of the noncoordinating residues of the reduced T3$\beta$ Cu in the variants. (The frozen $\alpha$-carbons limit the movement of the nonmutated His rings, preventing them from adapting the close-to-

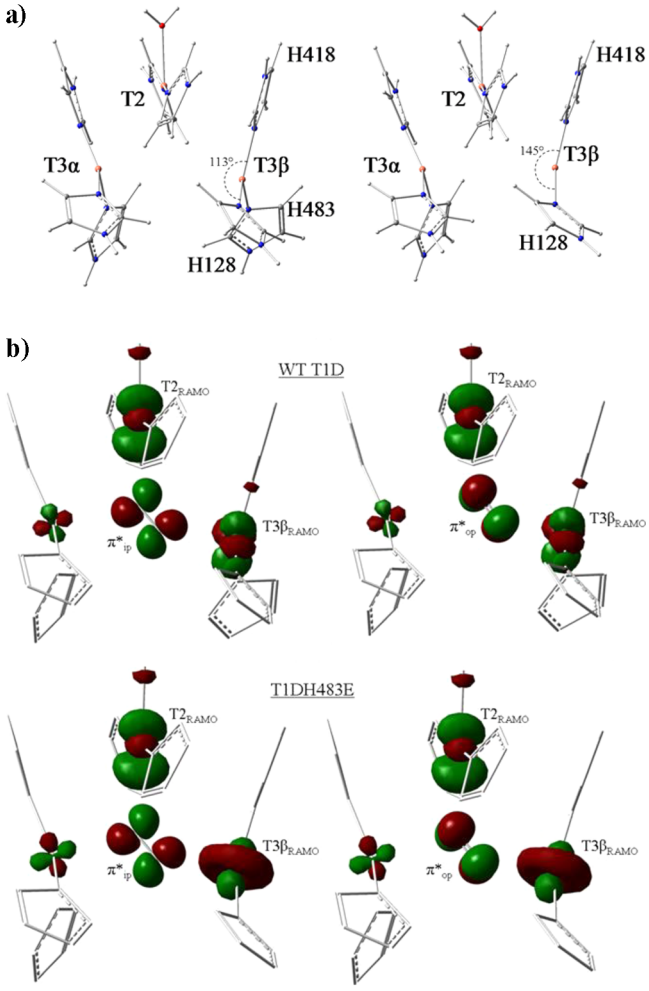


**Figure 10.** (a) Geometry optimized DFT structures of the three Cu ions and their coordinated His ligands in the TNC of WT (left) and H483E/Q (right) variants in Fet3p. (b) Interaction between the T2 and T3$\beta$ Cu RAMOs and the $\pi$*-in- and out-of-plane SOMOs of $O_2$, where the in-plane SOMO is in the T2, T3$\alpha$, and T3$\beta$ plane, and the out-of-plane SOMO is perpendicular to this plane.


dx.doi.org/10.1021/bi4002826 | Biochemistry 2013, 52, 3702−3711

linear arrangement observed experimentally.) Fast two-electron electron transfer to dioxygen by a binuclear Cu site (the T2 and T3$\beta$ Cu atoms in MCOs) requires good initial orbital overlap of the highest occupied redox active molecular orbital (RAMO) of each Cu, with the two half occupied perpendicular $\pi$*-orbitals of $O_2$. Figure 10b shows the DFT determined contours of the T2 and T3$\beta$ Cu RAMOs of the WT enzyme (top) and the variant (bottom). No change is observed for the T2 Cu RAMO between the WT enzyme and the variants, both providing $\sigma$-bonding capability (with the in-plane $\pi^*_{ip}$ of $O_2$) toward the interior of the TNC. However, due to the increase in the N−Cu−N angle, the T3$\beta$ Cu RAMO of the variants has $d_{z^2}$ character and thus $\sigma$-bonding capability, as opposed to the $d_{xy}$ RAMO of the WT T3$\beta$ Cu, which has $\pi$ -bonding capability toward the interior of the TNC. The TNC in the WT enzyme is therefore set up for bonding interactions with each of the perpendicular $\pi$*-$\beta$-spin unoccupied molecular orbitals (SOMOs) of $O_2$ ($\pi_{ip}$* in Figure 10b top, left ,and $\pi_{op}$* in Figure 10b top, right). In contrast, the H483 variants only provide $\sigma$-bonding interactions, via the T2 and T3$\beta$ Cu RAMOs with the $O_2$, that are in the same plane, and therefore interact with only one $\pi$*-orbital of the $O_2$ ($\pi_{ip}$* in Figure 10b bottom, left). For $O_2$ to accept two electrons into the same $\pi$*-orbital, it must be promoted into the singlet state (from the triplet ground state), which is not energetically favorable. Thus, mutating the H483 ligand of the T3$\beta$ Cu strongly affects the geometric and electronic structure of the reduced TNC, which in the wild type enzyme is setup for fast two-electron reduction of dioxygen to form a bridged peroxide intermediate in the first half of the reaction cycle.

## 4. SUMMARY

This study highlights the consequence of perturbing the innersphere coordination environment of the TNC in the MCOs, with respect to the rate determining first two-electron reduction of $O_2$. In the Fet3p variants T1DH483E and Q, the geometric and electronic structure only allows for a slow one-electron oxidation of the T3$\beta$ Cu. In contrast, the geometric and electronic structure of the TNC in the WT enzyme allows for $O_2$ to bridge with efficient overlap of the T2 and T3$\beta$ Cu RAMOs with the two perpendicular $\pi$*-SOMOs of triplet $O_2$. This results in effective two-electron reduction to form a bridged PI structure, as required for reductive cleavage of the O−O bond.

## ■ ASSOCIATED CONTENT

### Supporting Information

Spectroscopic characterization of as-isolated holo H483E, including room-temperature absorbance, EPR, and Cu K-edge spectra; redox titration of Holo H483E followed by absorbance and EPR; EPR Simpow fits of intermediate and resting forms of T1DH483E; modeling of Cu K-edge XAS spectrum of reduced T1DH483E; Cu K-edge spectra of reduced, and reoxidized (~30 s) T1DH483Q; data and fit of reoxidation of T1DH483Q evaluated by spin integrated EPR intensity; and cartoon representation of TNC structure of Fet3p. This material is available free of charge via the Internet at http://pubs.acs.org.

## ■ AUTHOR INFORMATION

### Corresponding Authors

*(D.J.K.) Phone: (716) 829-2842. E-mail: camkos@buffalo.edu.

*(E.I.S.) Phone: (650) 723-9104. E-mail: Edward.Solomon@stanford.edu.

### Funding

This research was supported by NIH Grants DK-31450 (to E.I.S.), DK53820 (to D.J.K), and RR-001209 (to K.O.H). Portions of this research were carried out at the Stanford Synchrotron Radiation Lightsource, a Directorate of SLAC National Accelerator Laboratory and an Office of Science User Facility operated for the U.S. Department of Energy Office of Science by Stanford University. The SSRL Structural Molecular Biology Program is supported by the DOE Office of Biological and Environmental Research, and by the National Institutes of Health, National Center for Research Resources, Biomedical Technology Program. C.H.K. is a Stanford Graduate Fellow.

### Notes

The authors declare no competing financial interest.

## ■ REFERENCES

(1) Blanford, C. F., Heath, R. S., and Armstrong, F. A. (2007) A stable electrode for high-potential, electrocatalytic O-2 reduction based on rational attachment of a blue copper oxidase to a graphite surface. *Chem. Commun.*, 1710−1712.

(2) Reinhammar, B. (1972) Oxidation-reduction potentials of electron acceptors in laccases and stellacyanin. *Biochim. Biophys. Acta 275*, 245−259.

(3) Solomon, E. I., Sundaram, U. M., and Machonkin, T. E. (1996) Multicopper oxidases and oxygenases. *Chem. Rev. 96*, 2563−2605.

(4) Claus, H. (2003) Laccases and their occurrence in prokaryotes. *Arch. Microbiol. 179*, 145−150.

(5) Gutteridge, J. M. C., and Stocks, J. (1981) Ceruloplasmin-physiological and pathological perspectives. *Crit. Rev. Clin. Lab. Sci. 14*, 257−329.

(6) Kosman, D. J. (2003) Molecular mechanisms of iron uptake in fungi. *Mol. Microbiol. 47*, 1185−1197.

(7) Thurston, C. F. (1994) The structure and function of fungal laccases. *Microbiology 140*, 19−26.

(8) Giardina, P., Faraco, V., Pezzella, C., Piscitelli, A., Vanhulle, S., and Sannia, G. (2010) Laccases: a never-ending story. *Cell. Mol. Life Sci. 67*, 369−385.

(9) Addleman, K., and Archibald, F. (1993) Kraft pulp bleaching and delignification by dikaryons and monokaryons of *Trametes versicolor*. *Appl. Environ. Microbiol. 59*, 266−273.

(10) Mayer, A. M., and Staples, R. C. (2002) Laccase: new functions for an old enzyme. *Phytochemistry 60*, 551−565.

(11) Christenson, A., Shleev, S., Mano, N., Heller, A., and Gorton, L. (2006) Redox potentials of the blue copper sites of bilirubin oxidases. *Biochim. Biophys. Acta, Bioenerg. 1757*, 1634−1641.

(12) Mano, N., Kim, H. H., Zhang, Y. C., and Heller, A. (2002) An oxygen cathode operating in a physiological solution. *J. Am. Chem. Soc. 124*, 6480−6486.

(13) Solomon, E. I., Augustine, A. J., and Yoon, J. (2008) O(2) Reduction to H(2)O by the multicopper oxidases. *Dalton Trans.*, 3921−3932.

(14) Solomon, E. I., Ginsbach, J. W., Heppner, D. E., Kieber-Emmons, M. T., Kjaergaard, C. H., Smeets, P. J., Tian, L., and Woertink, J. S. (2011) Copper dioxygen (bio) inorganic chemistry. *Faraday Discuss. 148*, 11−39.

(15) Gewirth, A. A., and Solomon, E. I. (1988) Electronic-structure of plastocyanin- excited state spectral features. *J. Am. Chem. Soc. 110*, 3811−3819.

(16) Cole, J. L., Clark, P. A., and Solomon, E. I. (1990) Spectroscopic and chemical studies of the laccase trinuclear active-site- geometric and electronic structure. *J. Am. Chem. Soc. 112*, 9534−9548.

(17) Solomon, E. I., Chen, P., Metz, M., Lee, S. K., and Palmer, A. E. (2001) Oxygen binding, activation, and reduction to water by copper proteins. *Angew. Chem., Int. Ed. 40*, 4570−4590.

(18) Rulisek, L., Solomon, E. I., and Ryde, U. (2005) A combined quantum and molecular mechanical study of the O-2 reductive cleavage in the catalytic cycle of multicopper oxidases. *Inorg. Chem. 44*, 5612−5628.
(19) Aasa, R., Branden, R., Deinum, J., Malmstrom, B. G., Reinhammar, B., and Vanngard, T. (1976) Paramagnetic intermediate in reduction of oxygen by reduced laccse. *FEBS Lett. 61*, 115−119.
(20) Lee, S. K., George, S. D., Antholine, W. E., Hedman, B., Hodgson, K. O., and Solomon, E. I. (2002) Nature of the intermediate formed in the reduction of O-2 to H2O at the trinuclear copper cluster active site in native laccase. *J. Am. Chem. Soc. 124*, 6180−6193.
(21) Yoon, J., and Solomon, E. I. (2007) Electronic structure of the peroxy intermediate and its correlation to the native intermediate in the multicopper oxidases: Insights into the reductive cleavage of the O-O bond. *J. Am. Chem. Soc. 129*, 13127−13136.
(22) Augustine, A. J., Kjaergaard, C., Qayyum, M., Ziegler, L., Kosman, D. J., Hodgson, K. O., Hedman, B., and Solomon, E. I. (2010) Systematic perturbation of the trinuclear copper cluster in the multicopper oxidases: the role of active site asymmetry in its reduction of O(2) to H(2)O. *J. Am. Chem. Soc. 132*, 6057−6067.
(23) Palmer, A. E., Quintanar, L., Severance, S., Wang, T. P., Kosman, D. J., and Solomon, E. I. (2002) Spectroscopic characterization and O-2 reactivity of the trinuclear Cu cluster of mutants of the multicopper oxidase Fet3p. *Biochemistry 41*, 6438−6448.
(24) Cole, J. L., Tan, G. O., Yang, E. K., Hodgson, K. O., and Solomon, E. I. (1990) Reactivity of the laccase trinuclear copper active-site with dioxygen- an X-ray absorption-edge study. *J. Am. Chem. Soc. 112*, 2243−2249.
(25) Palmer, A. E., Lee, S. K., and Solomon, E. I. (2001) Decay of the peroxide intermediate in laccase: Reductive cleavage of the O-O bond. *J. Am. Chem. Soc. 123*, 6591−6599.
(26) Shin, W., Sundaram, U. M., Cole, J. L., Zhang, H. H., Hedman, B., Hodgson, K. O., and Solomon, E. I. (1996) Chemical and spectroscopic definition of the peroxide-level intermediate in the multicopper oxidases: Relevance to the catalytic mechanism of dioxygen reduction to water. *J. Am. Chem. Soc. 118*, 3202−3215.
(27) Bradford, M. M. (1976) Rapid and sensitive method for quantitation of mcrogram quantities of protein utilizing the principle of protein-dye binding. *Anal. Biochem. 72*, 248−254.
(28) Felsenfeld, G. (1960) The determination of cuprous ion in copper proteins. *Arch. Biochem. Biophys. 87*, 247−251.
(29) Nilges, M. J., Mattson, K., and Belford, R. L. (2007) Simpow6: A software package for the simulation of esr powder-type spectra. *ESR Spectrosc. Membr. Biophys. 27*, 261−281.
(30) Tenderholt, A., Hedman, B., and Hodgson, K. O. (2006) PySpline: A modern, Cross-Platform Program for the Processing of Raw Averaged XAS Edge and EXAFS Data, in *13th International Conference on X-Ray Absorption Fine Structure (XAFS13)*, pp 105−107, American Institute of Physics, Stanford, CA.
(31) Frisch, M. et al. (2009) *Gaussian 09*, Gaussian, Inc., Wallingford, CT. See Supporting Information for the complete reference.
(32) Kau, L. S., Spirasolomon, D. J., Pennerhahn, J. E., Hodgson, K. O., and Solomon, E. I. (1987) X-ray abdorption-edge determination of the oxidation-state and coordiantion-number of copper- application to the type-3 site in *Rhus vernicifera* laccase and its reaction with oxygen. *J. Am. Chem. Soc. 109*, 6433−6442.
(33) Taylor, A. B., Stoj, C. S., Ziegler, L., Kosman, D. J., and Hart, P. J. (2005) The copper-iron connection in biology: Structure of the metallo-oxidase Fet3p. *Proc. Natl. Acad. Sci. U.S.A. 102*, 15459−15464.
(34) Gewirth, A. A., Cohen, S. L., Schugar, H. J., and Solomon, E. I. (1987) Spectroscopic and theoretical-studies of the unusual electron-paramagnetic-res parmeters of distorted tetrahedral cupric sites-correlations to X-ray spectraal features of core levels. *Inorg. Chem. 26*, 1133−1146.
(35) Quintanar, L., Yoon, J. J., Aznar, C. P., Palmer, A. E., Andersson, K. K., Britt, R. D., and Solomon, E. I. (2005) Spectroscopic and electronic structure studies of the trinuclear Cu cluster active site of the multicopper oxidase laccase: Nature of its coordination unsaturation. *J. Am. Chem. Soc. 127*, 13832−13845.
(36) Chen, P., Fujisawa, K., and Solomon, E. I. (2000) Spectroscopic and theoretical studies of mononuclear copper(II) alkyl- and hydroperoxo complexes: Electronic structure contributions to reactivity. *J. Am. Chem. Soc. 122*, 10177−10193.
(37) Freeman, A. J., and Watson, R. E. (1965) Hyperfine Interactions in Magnetic Materials, in *Magnetism*, pp 168−305305, Academic Press, New York.
(38) Holm, R. H., Kennepohl, P., and Solomon, E. I. (1996) Structural and functional aspects of metal sites in biology. *Chem. Rev. 96*, 2239−2314.
(39) Wood, P. M. (1988) The potential diagram for oxygen at pH-7. *Biochem. J. 253*, 287−289.